Chapter 2

Reduced Graphene Oxide – Zinc Sulfide ($RGO - ZnS$) Composite for Solar Light Responsive Photo Current Generation and Photocatalytic 4-Nitrophenol Reduction

2.1 Introduction

Photocurrent generation in the solar spectrum region is of great significance for a variety of applications in the field of solar cell, photodetectors, sensors, and environmental research [172-176]. Now a days, reduced graphene oxide (RGO) based composite materials are considered as building blocks for optoelectronic application owing to its excellent photo induced charge generation in solid phase as well as in the solution phase [176-182]. In these systems RGO provides an excellent support to anchor different optical materials on its basal plane, which facilitates the separation of photoinduced charge efficiently and subsequently increases the optoelectronic activity of the composite [177-182]. In RGO based composites, the photo induced electrons migrate to RGO sheets from the conduction band of the attached optical materials that hinder the electron–hole recombination possibility and increases the photogenerated charge carrier concentration. Several approaches have been proposed to tailor different RGO based composites to cater the active material for optoelectronic devising [180-186]. Most of the reports focus on RGO based oxide semiconductors composite, whose performance is strongly impaired by the oxygen vacancies and surface absorption–desorption processes which causes photocurrent instability [187]. To overcome this limitation, researchers have developed metal chalcogenide semiconductor-RGO composites for optoelectronic applications. So far, a few semiconducting chalcogenide based RGO composites such as $RGO - CdS$ [184], $RGO - Cu_2S$ [185], $RGO - CdZnS$ [132], $RGO - PbS$ [225] were synthesized and used for different optoelectronic applications through photoinduced charge generation.

To this end, Zinc Sulfide (ZnS), a wide band gap ($3.7\,eV$) semiconductor, has shown outstanding transport properties, high thermal stability and good electronic mobility [188-190]. The fast generation of photoinduced excitons and the high negative reduction potential of excited electrons makes ZnS a potential candidate for optoelectronic and photocatalytic applications [191]. Due to these excellent optoelectronic properties, efforts have been made to prepare RGO–ZnS composites with multifunctionality. For example, Song et al. reported a high photocurrent generation in $RGO-CdSe/ZnS$ composite synthesized by ionic liquids [192]. Researchers have already reported $RGO-ZnS$ composites exhibiting excellent photocatalytic activity [188, 193, 222]. The in-depth study of ac conductivity of $RGO-ZnS$ composite indicates the occurrence of phonon-assisted simple quantum tunneling of electrons between the defects present in RGO [195]. All of the above studies are confined within the application of $RGO-ZnS$ composite in the UV region either for photocurrent generation or photocatalytic degradation of organic dyes only. Whereas, the photocurrent generation in $RGO-ZnS$ thin film devices or photocatalytic degradation of other toxic water pollutant under solar light irradiation remains unexplored.

Nitro phenols have attracted great attention in recent studies as they are considered a priority among toxic environmental pollutants [196]. Increased agricultural and industrial activity has resulted in a proportional growth in pesticide usage which, in turn, has seen to the global growth of phenols in the environment [197]. Phenols are a hazard to the environment for its high toxicity and persistence in water and is difficult to remove it from groundwater due to its high stability and solubility in water [196, 197]. Photocatalytic

degradation of phenol and its derivatives are highly desirable in environmental aspects.

Figure 2.1.1: Schematic diagram of Applications of RGO-ZnS

Herein we report the photocurrent generation and photocatalytic activity of one-step solvothermally synthesized $RGO - ZnS$ composite. We have investigated the solar light responsive photocurrent generation in $RGO-ZnS$ composite in solid, as well as solution phase. The X-ray Diffraction (XRD) and High Resolution Transmission Electron Microscopy ($HRTEM$) indicate that the ZnS nanorods are highly crystalline. The reduction of graphene oxide (GO) to RGO was confirmed by X-ray Photoelectron spectroscopy (XPS) analysis. The optical properties were characterized by $UV-vis$ and $FTIR$ spectroscopy. The $RGO - ZnS$ thin film device depicts an excellent

photocurrent generation under simulated solar light irradiation, with the linear variation of photosensitivity with intensity. We have also extended the application of the $RGO - ZnS$ composite to remove the toxic organic water pollutant 4-nitrophenol ($4-NP$) by the photocatalytic reduction under solar light illumination. Our observations established the promise of the $RGO - ZnS$ composite towards the removal of $4 - NP$ from an aqueous medium under solar radiation. Thus the $RGO - ZnS$ composite serves as an efficient photo detector as well as an excellent anti pollutant for water purification.

2.2 Experimental Section

2.2.1 Materials Used

Graphite, potassium persulfate [$K_2S_2O_8$], phosphorus pentoxide [P_2O_5], sodium nitrate [$NaNO_3$], potassium permanganate [$KMnO_4$], zinc acetate dihydrate [$Zn(CH_3COO)_2, 2H_2O$] and thiouria [NH_2CSNH_2] were purchased from Sigma-Aldrich and sulphuric acid [H_2SO_4], hydrogen peroxide [H_2O_2], hydrochloric acid [HCl], ethylenediamine [$EN, NH_2CH_2CH_2NH_2$], 4-nitrophenol [$4-NP$] and sodium borohydride [$NaBH_4$] were purchased from Merck. All the chemicals were used as received.

2.2.2 Materials Synthesis

2.2.2.1 Preparation of *GO*

GO was prepared from purified natural graphite powder by the modified Hummers method [172]. As typical to this process, $2\,gm$ of Graphite powder, $1\,gm$ of $K_2S_2O_8$ and $1\,gm$ of P_2O_5 were added to $20\,mL$ of 98% H_2SO_4 at $80°C$ and the mixture was kept under stirring for $6\,h$. After that, the graphite powder **(called as preoxidized graphite)**, was washed several times with distilled water (DW) and dried at $60°C$.

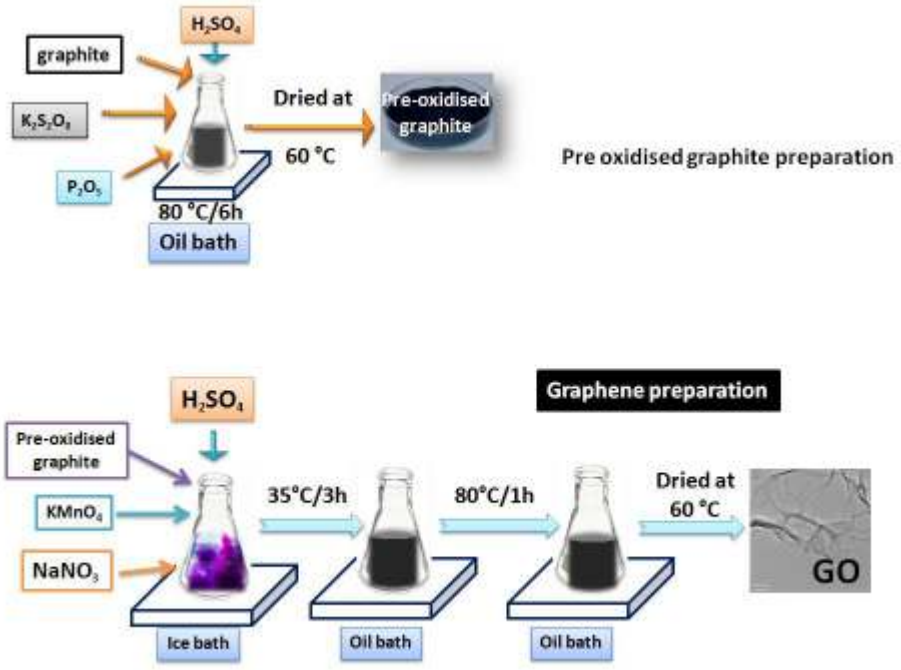

Figure 2.2.1: Preoxidized graphite and GO synthesis

$0.2\,gm$ of as-prepared preoxidized graphite powder and $0.1\,g$ of $NaNO_3$ were added to $5\,mL$ concentrated H_2SO_4 in an ice-bath below $5°C$, and then $0.6\,gm$ of $KMnO_4$ was added slowly under stirring condition. The

mixture was then allowed to reach at room temperature and transferred to a preheated bath at $35°C$ and kept for another $3\,h$ and followed by the addition of $40\,mL$ of DW slowly to the mixture. The temperature of the mixture was maintained at $80°C$ for $1\,h$ by introducing external heating arrangement. $12\,mL$ of $3\,wt\%$ of H_2O_2 solution was added to terminate the reaction and GO was synthesized. The volume of the mixture was increased to $100\,mL$ by adding DW, and the mixture was kept under stirring condition for the next $12\,h$. To remove the metallic ions in GO, a dilute HCl $[H_2O : HCl = 10 : 1]$ solution was added to the GO solution and kept under stirring condition for $5\,h$. The GO thus synthesized, was washed with DW until the pH reached 6 and dried at $60°C$ overnight.

2.2.2.2 Synthesis of controlled RGO, controlled-ZnS and the $RGO - ZnS$ nanocomposite

The reduction of GO to RGO, synthesis of controlled-ZnS nanorod and the synthesis of $RGO-ZnS$ nanocomposite were done by simple solvothermal reaction. For synthesis of $RGO-ZnS$ nano composite, $1.65\,g$ of $Zn(CH_3COO)_2, 2H_2O$ and $1.14\,g$ of NH_2CSNH_2 were dissolved in a $36\,mL$ solution of EN and DW $(1 : 1$ volume ratio). Then $80\,mg$ of GO powder was added slowly to the solution under stirring condition, followed by sonication for 15 min to get a homogeneous mixture. The mixture was then transferred in a Teflon-lined stainless steel autoclave of volume $60\,mL$. Up to 60% of the total volume of the autoclave was filled with the mixture. The autoclave was sealed appropriately and put in a preheated oven maintained at $170°C$ and the reaction was continued for $18\,h$. Then the autoclave was allowed to cool down au-

tomatically to room temperature in next $12\,h$. After reaching the normal temperature, synthesized $RGO - ZnS$ composite was collected and washed with DW and ethanol for several times by centrifugation followed by dried at $60°C$ in a vacuum oven for $12\,h$. Controlled-ZnS nanorod and RGO were synthesized as controlled sample by using a similar experimental protocol where for synthesis of ZnS nanorod GO is absennt and for the synthesis of RGO Zinc Acetate Dihydrate and Thiourea are absent.

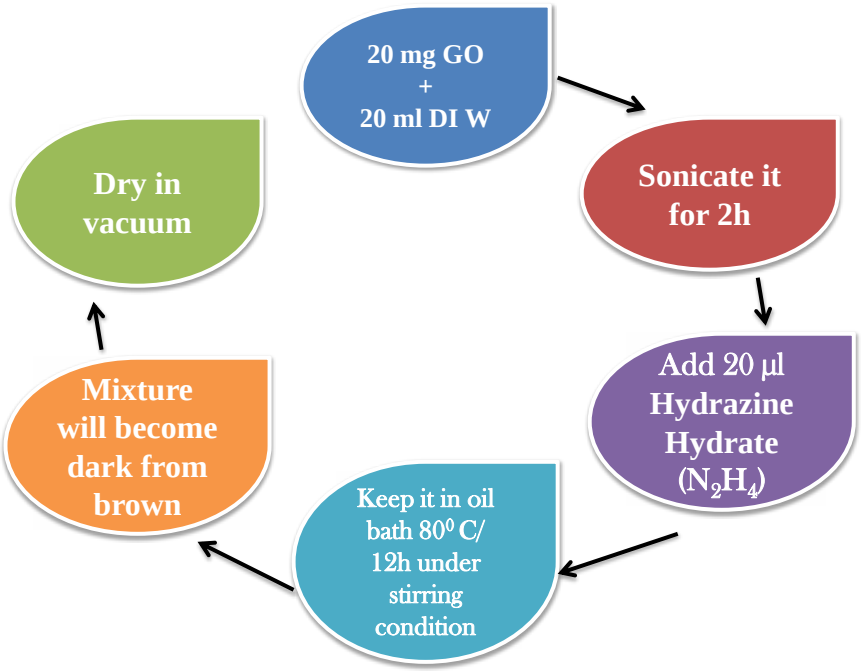

Figure 2.2.2: Synthesis of RGO

2.3 Materials Characterisation

The overall crystalinity of the synthesized materials were examined by the X-ray diffraction (XRD, Rigaku Miniflex, Japan), with a $Cu\ K_\alpha$ radiation.

Detailed micro morphology and crystal structures of the composite were obtained from transmission electron microscope (TEM) and high-resolution TEM ($HRTEM$) studies, ($JEOL$ 2010, operated at $200\,kV$). The specimens were prepared by drop casting the $RGO-ZnS$ dispersion onto a carbon-coated 300 mesh copper grid and dried under room temperature. The XPS data was recorded on an $ULVAC-PHI$ 5000 Versa Probe II spectroscope using a monochromater $Al\ K_\alpha$ ($1486.6\,eV$), source operated at a voltage of $15\,kV$ and $25\,W$. The chamber pressure was kept below 10^{-10} torr. The pass energy was set at 117.4 and $29.35\,eV$ for survey and high resolution spectra respectively. The Fourier transform infrared ($FTIR$) spectra were recorded on a $FTIR$ spectrometer (Perkin Elmer Spectrum 100) with a resolution of $1\,cm^{-1}$. The $UV-visible$ spectra were obtained on an $UV-visible$ Spectrophotometer (Shimadzu $UV-1700$) at room temperature. The steady state photoluminescence (PL) studies were performed in Fluorescence spectrophotometer (Perkin Elmer $LS\,55$) at room temperature.

2.3.1 Photocurrent generation in $RGO-ZnS$ thin film device

The photocurrent generation was studied by fabricating a thin film device on a pre-cleaned glass substrate, by drop casting the $RGO-ZnS$ composite dispersed in isopropyl alcohol. Conducting silver paint was used to draw two parallel electrodes on the $RGO-ZnS$ thin film. The current (I) – voltage (V) characteristics under dark and illuminated conditions were carried out by a Keithley $2612A$ sourcemeter, in ambient conditions. Data was collected

by Lab Tracer 2.0 interfaced with the data acquisition card and a solar light simulator (Oriel 67005, Newport) was used to illuminate the thin film device.

2.3.2 Photocatalytic reduction of $4-NP$ in presence of $RGO-ZnS$

To study the photocatalytic reduction of $4-NP$ ($0.3\times10^{-4}M$), a $250\,mL$ glass photoreactor equipped with solar-light simulator (Oriel 67005, Newport) was employed as the illumination source ($AM1.5, 100\,mW/cm^2$), in the presence of $2\,g/L$ catalyst at $300\,K$ together with addition of $5\,mL$ of $NaBH_4$ ($1.0\times10^{-1}M$) under constant stirring. The yellow color of the solution disappeared gradually, representing the reduction of $4-NP$ during the photocatalytic process. Samples were directly collected from the photoreactor in a regular interval of ($5\,min$) illumination followed by measuring UV–vis absorption spectra by using a Shimadzu UV-1700 spectrophotometer. The decrease of absorption peak intensity (at $400\,nm$) of phenolet ion (produced in alkali medium) with the illumination time was monitored to study the photo reduction of $4-NP$. At the end of the reaction, the $RGO-ZnS$ composite was separated from the degraded product by centrifugation several times and the process was repeated to check the stability of the catalyst.

2.4 Results and Discussion

The XRD patterns of synthesized GO, RGO, controlled-ZnS nanorod and the $RGO-ZnS$ composites are shown in Figure 2.4.1A. The signature peak

of GO (2θ= 10.4^0), corresponding to a graphitic (002) plane with interplanar spacing of $0.85\,nm$. The (002) peak completely disappears and a very broad diffraction peak at 2θ value of 25.0^0 appears after solvothermal reduction of GO. The peaks of controlled ZnS and $RGO-ZnS$ composite can readily be indexed to the standard values of the hexagonal wirtzite (JCPDS $36-1450$) ZnS structure. Moreover, no diffraction peaks for RGO can be observed in the $RGO-ZnS$, might be due to the low diffraction intensity of RGO in the composite with respect to the controlled- ZnS nanorod.

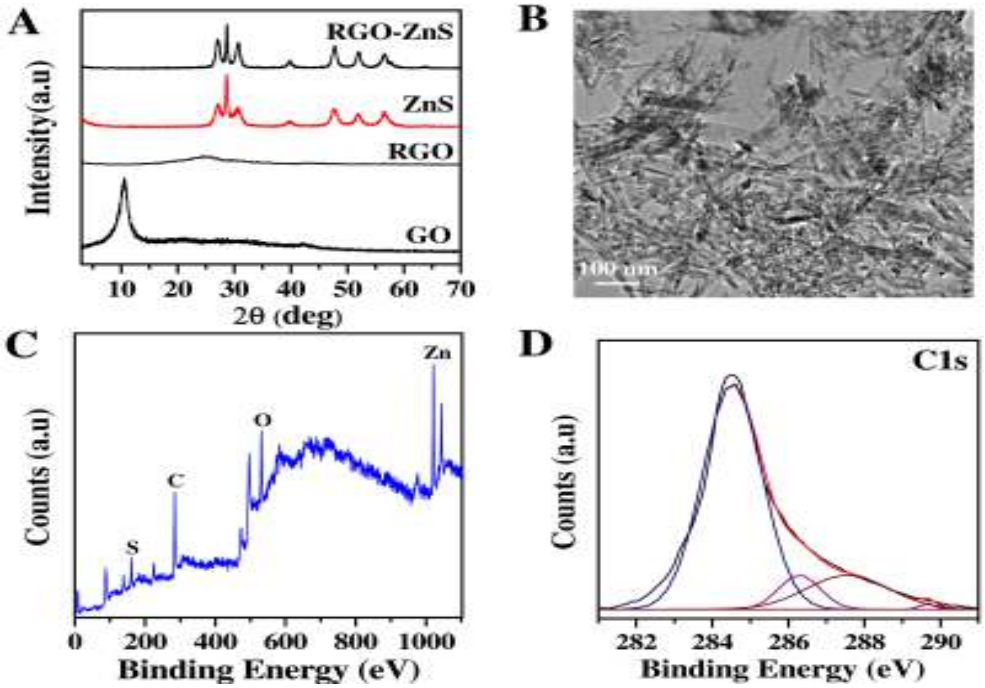

Figure 2.4.1: (A) The XRD patterns of GO, ZnS nanorod and $RGO-ZnS$ composite. (B) TEM images of $RGO-ZnS$ composite. (C) XPS survey scan of $RGO-ZnS$ composite. (D) High resolution XPS spectra with C $1\,s$ peak deconvolution of $RGO-ZnS$ composite.

TEM analysis was performed to study the microscopic structure of the $RGO-ZnS$ composite and is presented in Figure 2.4.1B. The RGO nanosheets

are covered with ZnS nanorods of average length and diameter of $40-50$ and $8-10\,nm$ respectively. The $HRTEM$ analysis [Figure 2.4.2], depicts that the ZnS nanorods in $RGO-ZnS$ have high crystalinity with well resolved lattice spacing ($0.31\,nm$) of ZnS, oriented along (002) lattice plane.This value is equal to that of the value calculated from the XRD analysis. It is also clearly observed that the ZnS nanorods were supported intimately on the surface of RGO sheets. This intimate support increases the possibility of the electronic interaction between ZnS and RGO that facilitates the charge separation and the photocatalytic activity. The nanorod morphology will also provide favorable condition for efficient charge transfer due to its better crystallinity[132]

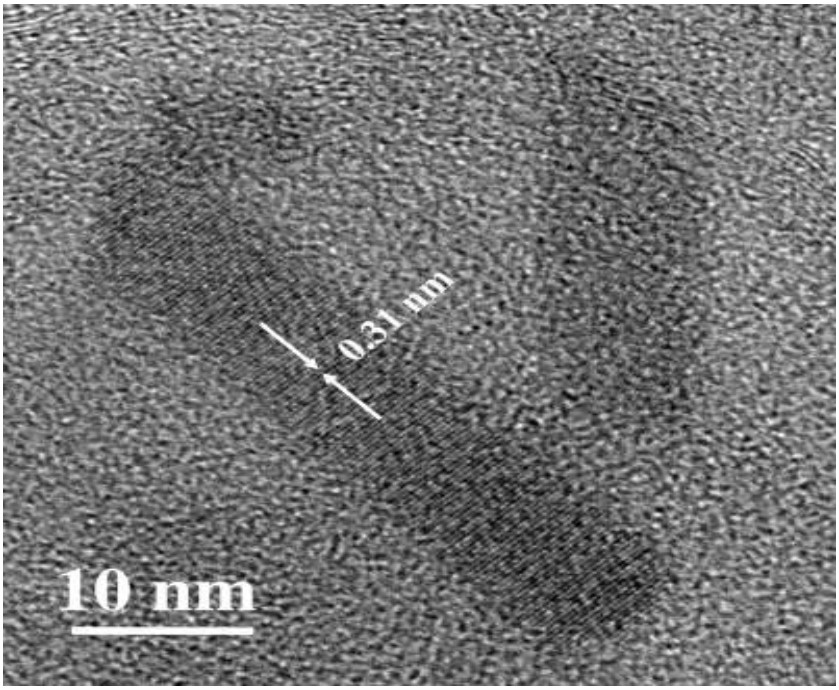

Figure 2.4.2: $HRTEM$ images of ZnS nanorod attached on RGO

XPS is a surface analytical technique that can provide useful informa-

tion on the nature of the functional groups and the chemical composition of surfaces. Figure 2.4.1C shows the XPS survey spectrum of the RGO–ZnS composite, which establishes the coexistence of Zn, C, O and S. The deconvolution of the $C\,1s$ peak of the synthesized $RGO-ZnS$ is shown in Figure 2.4.1D. The integrated peak area corresponding to the sp^2 bonded carbon $(C-C)$ peak at $284.5\,eV$ is of $8\,to\,10$ times higher than that of C–OH $(286.6\,eV)$, C–O $(287.4\,eV)$ and O–$C=O$ $(288.9\,eV)$ bonds. The relatively low intensity of the oxygenated groups in $RGO-ZnS$, proves the effective reduction of GO by the amino groups present in Ethylendiamine (EN) and thiourea by the solvothermal process [195, 198]. The XPS analysis also depicts that effective reduction of GO in this system is about 80%. The high resolution XPS spectra of O, Zn and is shown in Figure 2.4.3.

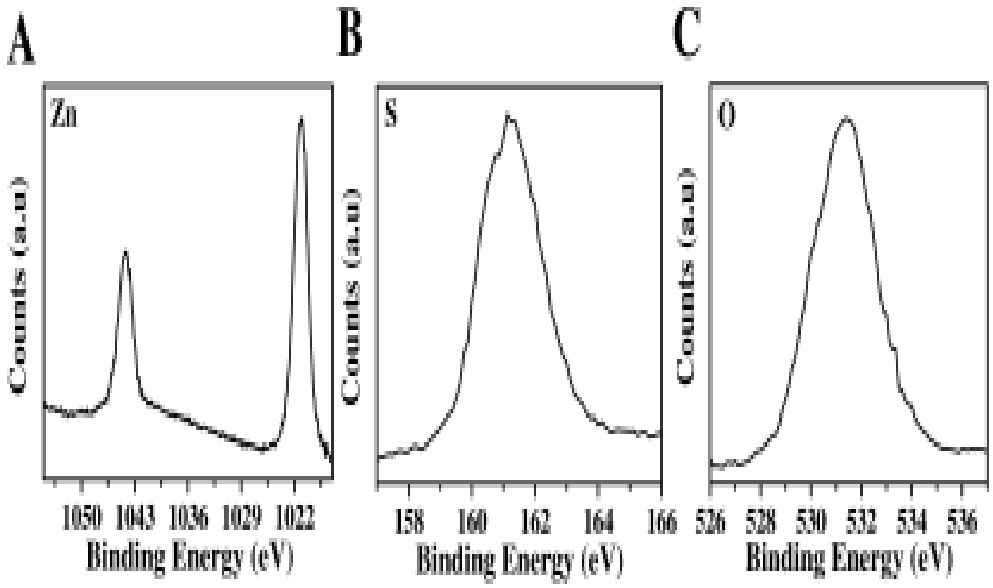

Figure 2.4.3: High resolution XPS spectra of (A) Zn. (B) S. (C) O.

The successful reduction of GO and the formation of $RGO-ZnS$ com-

posite was further confirmed by $FTIR$ spectroscopy. The $FTIR$ spectra of GO, ZnS and the RGO–ZnS composite over the range of 500–4000 cm^{-1} are shown in Figure 2.4.4A. The broad and strong absorption peak of GO at around 3376 cm^{-1} corresponds to the stretching vibrations of hydroxyl groups. The other signature peaks of GO observed at 1042, 1224, 1402 and 1734 cm^{-1} are assigned to C–O stretching vibrations of epoxy groups, C–O stretching vibrations of phenolic C–OH, O–H deformation vibrations of tertiary C–OH, and $C = O$ stretching vibrations of $COOH$ groups respectively. The peak at 1620 $cm^{-1}$is associated to the H–O–H bending band of the moisture present in the GO or to the skeletal vibrations of unoxidized C–C bonding[199]. The peak observed at 655 cm^{-1}, 1319 cm^{-1} and 1134 cm^{-1} in the $FTIR$ spectra of controlled ZnS is due to the $Zn - S$ bond of ZnS nanorod, $C - N$ stretching and CH_2 twisting respectively, the latter two absorption arises from the EN. Surprisingly, in the $FTIR$ spectrum of the RGO–ZnS composite, all the bands related to the oxygen-containing functional groups in GO nearly vanished, as shown in Figure 2.4.4A, which also indicates the reduction of GO. In addition to this, a new peak located at 1570 cm^{-1} arises from the skeletal vibration of the RGO. The optical properties of ZnS and $RGO-ZnS$ composite were probed by UV–vis spectroscopy and is shown in Figure 2.4.4B.

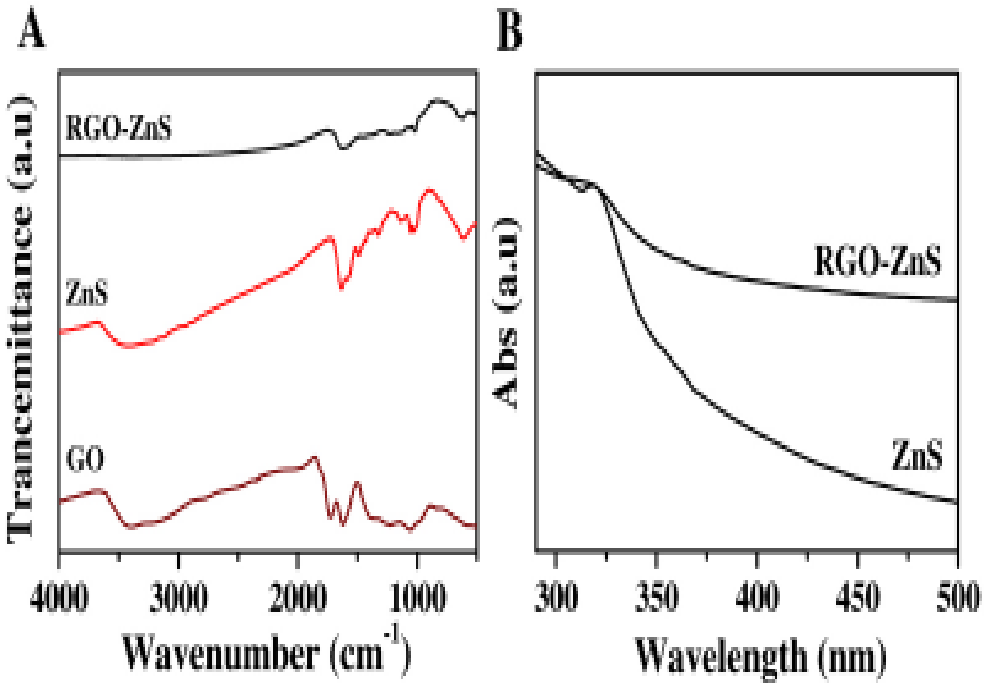

Figure 2.4.4: (A) $FTIR$ transmission spectra of GO, ZnS and $RGO - ZnS$ composite (B) $UV - vis$ absorption spectra of ZnS and $RGO - ZnS$ composite.

As expected, the controlled- ZnS shows the characteristic absorbance peak located at $330\,nm$ and the calculated value of direct band gap energy is $3.7\,eV$ (Figure 2.4.5).

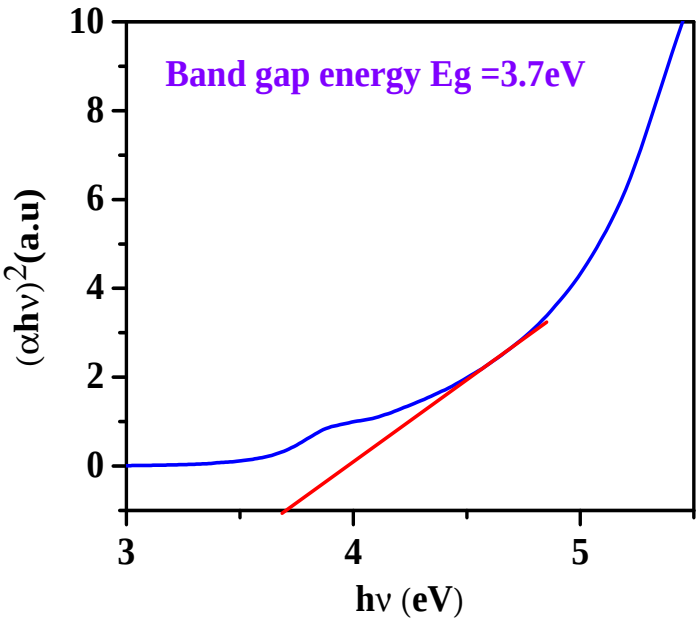

Figure 2.4.5: Band gap energy of ZnS material

It is clearly observed that the addition of RGO increases significantly the optical absorbance of $RGO - ZnS$ composite. The effective increase of the absorbance of the composite can be ascribed as the augment of surface electronic charge of the ZnS due to the incorporation of RGO [200, 201]. The absorption edge of $RGO - ZnS$ composite is similar to that of controlled-ZnS which indicates that RGO is not incorporated into the lattice of ZnS nanorod crystal [202]. In addition to this, a red shift in the absorption edge of $RGO-ZnS$ composite is observed as compared to controlled-ZnS, attributed to the chemical linkage between the RGO and ZnS [203].

To give significant insight into the photo induced charge generation and transfer at the interface of $RGO - ZnS$, the Photoluminescence (PL) study was performed at room temperature.

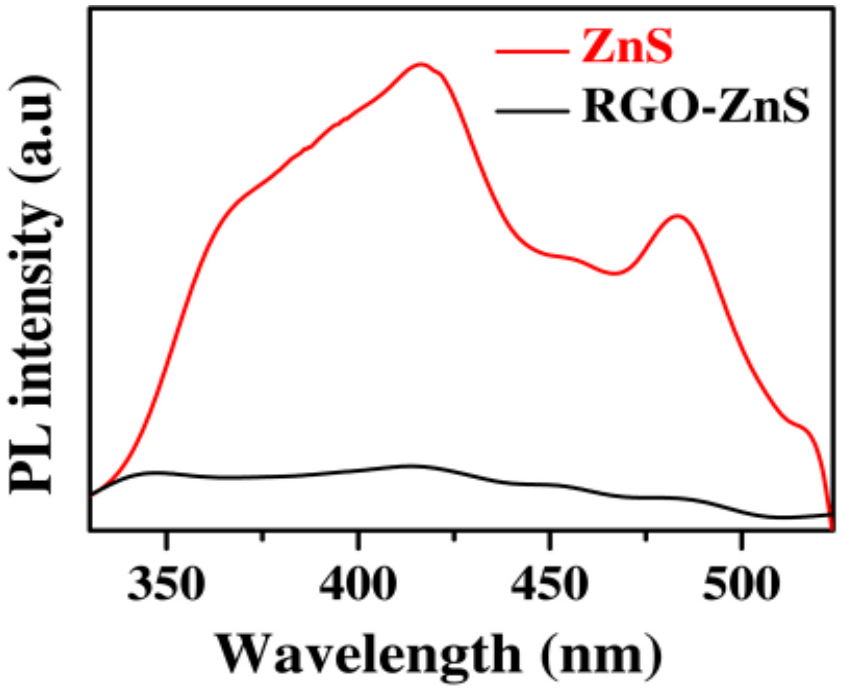

Figure 2.4.6: Photoluminescence spectra of controlled-ZnS and $RGO-ZnS$ composite

Figure 2.4.6 describes the PL spectrum of the controlled ZnS and $RGO-ZnS$ nanocomposites, excited at $280\,nm$ laser. A wide blue emission associated with an additional green emission is observed for controlled ZnS. Remarkably, the PL emission becomes quenched for $RGO-ZnS$, represents an effective interfacial charge-transfer process. Thus, it is expected that synthesize $RGO-ZnS$ composite have a potential applicability in optoelectronics field of application.

The optoelectronic transport of the fabricated device with $RGO-ZnS$ composite was investigated under dark and different illumination levels ($80-180\,mWcm^{-2}$). Figure 2.4.7A shows the cartoon of our thin film device along with electrical measurement setup. The $I-V$ characteristics under dark

and illuminated condition is displayed in Figure 2.4.7B. All the curves show linear variation of current with applied voltage and pass through the origin without showing any offset voltage. Linear variation of I with V indicates the formation of ohmic contact between the $RGO - ZnS$ composite film and the electrodes. The photocurrent (I_{Ph}) was calculated by subtracting the dark current (I_D) from current under illumination (I_L) [$I_{Ph} = I_L - I_D$]. Generation of photocurrent in a photodetector can be expressed as [204]:

$$I_{ph} = q\frac{\eta\tau_p P_{opt}}{Lh\nu}v_d = BP_{opt} \tag{2.4.1}$$

where, τ_p is the lifetime of photo induced carrier, q is the charge, v_d is the drift velocity, photon energy is $h\nu$, P_{opt} is the incident optical power, L is the length of the device and $B = q\frac{\eta\tau_p}{Lh\nu}v_d$ is the proportionality factor. The essential parameter, photosensitivity P (the ratio of I_{ph} to I_D), of the thin film device was also calculated. We have observed that I_{ph} increases linearly with the increase of light intensity, which leads to the linear variation of P with the illuminated light intensity (Figure 2.4.7C).

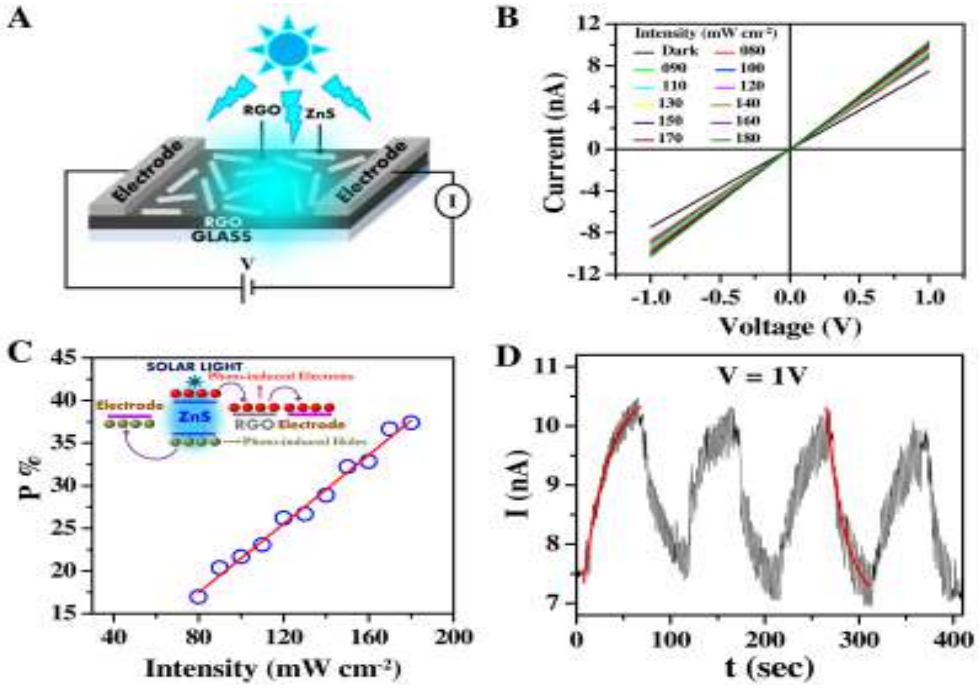

Figure 2.4.7: (A) The cartoon of our photodetector device along with the electrical transport measurement setup (B) $I-V$ characteristics for $RGO-ZnS$ nanocomposite thin film device under dark and different illumination intensity. (C) The variation of photo sensitivity with illumination intensity of our thin film device. The mechanism of photocurrent generation is shown in the inset. (D) The growth and decay of current with fitting of Eqn. 2.4.2 and 2.4.3 respectively, when the illuminated light was turned ON and OFF for four cycles.

P reaches a value of 37 % under the illuminated intensity of $180\,mWcm^{-2}$. This linear variation of P with intensity is advantageous to tune the optoelectronic device performance and paves the way for its application. When the thin film is illuminated by simulated solar light, electron-hole pairs are generated in ZnS, which subsequently dissociates into free electrons and holes. The free carriers have a tendency to recombine. Due to the favorable match of chemical potential, electrons will be transferred to highly conducting RGO sheets and will reach to positive electrodes through the interconnected RGO

sheets. On the other hand, the holes will transport to the negative electrode causing a generation of photo current under simulated solar light illumination. With the increase of illuminated light intensity, more and more photo induced charge carriers will be generated and the current will increase with the illuminated intensity. The mechanism of photo current generation of our device is shown in the inset of Figure 2.4.7C. We now investigate the dynamical photo response of our $RGO - ZnS$ thin film device. The device was illuminated periodically by chopping the simulated solar light source with a period of $100\,s$ and duty cycle of half. The growth and decay of current is shown in Figure 2.4.7D.When the device is exposed under illumination of intensity $180\,mWcm^{-2}$, the current increases from its dark value of $7.5\,nA$ to its saturation value of $10.4\,nA$. After turning off the light the current in the device recovers its initial dark value. Figure 2.4.7D also establishes the stability and the reproducibility of $RGO - ZnS$ device. The growth and decay current can be fitted with the relations (2.4.2) and (2.4.3) respectively.

$$I(t) = I_{dark} + A\left\{1 - e^{\frac{-(t-t_0)}{\tau_1}}\right\} \tag{2.4.2}$$

$$I(t) = I_{dark} + B\left\{e^{\frac{-(t-t_0)}{\tau_2}}\right\} \tag{2.4.3}$$

where, τ_1 and τ_2 are the time constants for growth and decay of current, t_0 is the time when the illumination was turned ON (growth) and OFF (decay), A and B are the scaling constants. The time constant of our device is calculated as $\tau_1 = 24\,s$ (growth) and $\tau_2 = 20\,s$ (decay) from the fit of the above equations to the experimental data, and is shown in Figure 2.4.7D as

solid lines.

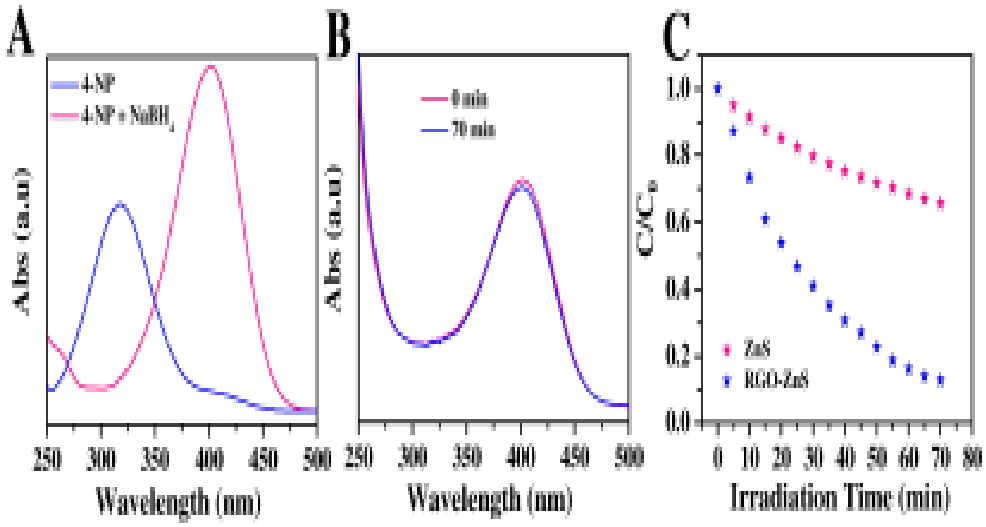

Figure 2.4.8: $UV-vis$ absorption spectrum of aqueous solution of (A) $4-NP$ and $4-NP$ with $NaBH_4$. (B) $4-NP$ and $NaBH_4$ without catalyst under dark. (C) Photocatalytic reduction of $4-NP$ under solar light irradiation with ZnS and $RGO-ZnS$ composites.

Recently, RGO-based composite photocatalysts have been utilized for photocatalytic degradation of different water pollutants [194, 205-207]. The photocatalytic reduction of $4-NP$ in presence of $NaBH_4$ is a standard protocol to probe the catalytic performance of different semiconducting catalyst [208, 209]. The $UV-vis$ absorption spectra of $4-NP$ in aqueous solution shows characteristics absorption peak at about $317\,nm$. Upon addition of $NaBH_4$, peak red shifted to $400\,nm$ owing to the formation of 4-nitrophenolate ion in alkali medium [$Figure\,2.4.8A$] [208-212]. Accordingly, the color of the solution changes from pale yellow to bright yellow. It was observed that in presence of $RGO-ZnS$, reduction process started immediately after shining of light and the characteristics absorption peak at $400\,nm$ gradually declines as the reaction time proceeds. However in absence

of any catalyst the peak intensity and position of phenolate ion remain unaffected for a long time both in dark and under simulated solar light, although $NaBH_4$ is considered as a strong reducing agent [208-212].[Figure 2.4.8B]

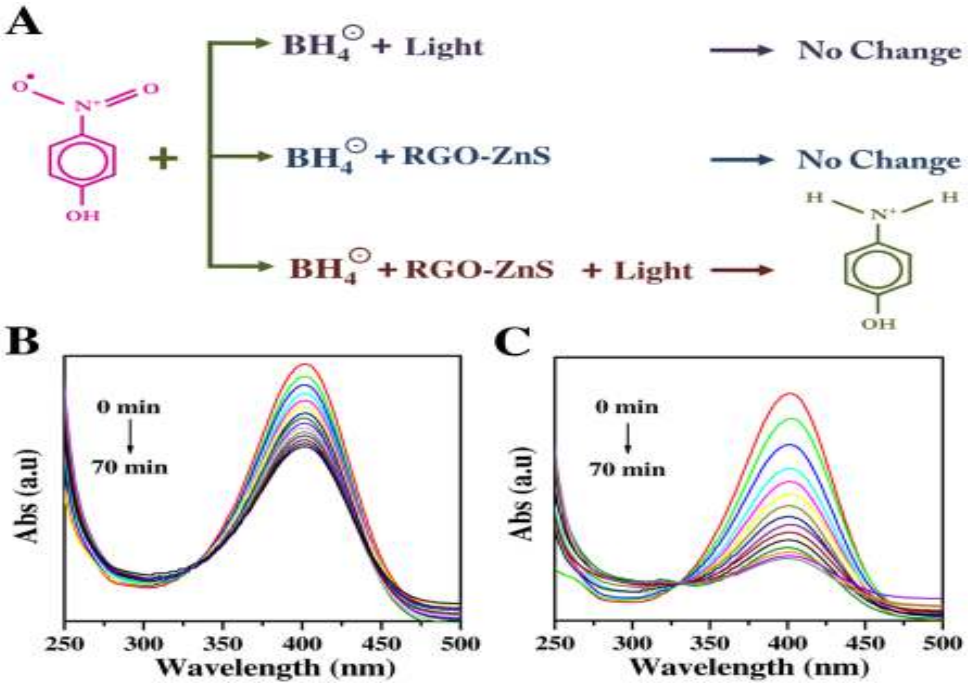

Figure 2.4.9: (A) Schematic representation of different reaction conditions for possible reduction of $4-NP$. $UV-vis$ absorption spectra of $4-NP$ in alkali medium with (B) controlled ZnS (C) $RGO-ZnS$ composite for different time of simulated solar light irradiation.

The weakening of the absorption peak intensity of nitrophenolate ion in presence of $RGO-ZnS$ was monitored over time under simulated light to evaluate the photocatalytic activity towards the reduction of $4-NP$. The photocatalytic activity under simulated solar light for controlled-ZnS and $RGO-ZnS$ composite, is presented in Figure 2.4.9B and 2.4.9C respectively.

The reduction efficiency is calculated as follows [81]:

$$DE\,(\%) \;=\; \left(1 - \frac{C}{C_0}\right) \times 100\% \tag{2.4.4}$$

where DE stands for Degradation Efficiency, C_0 represents the absorption peak intensity at time 0 (equivalent to the concentration of 4- NP), and C is the absorption peak intensity at different illumination intermissions (equivalent to the residual concentration of 4-NP). Figure 2.4.10A compares the reduction efficiency of $RGO - ZnS$ and ZnS under simulated solar light illumination. A illumination time of $70\,min$ was required to achieve 87% of reduction efficiency in presence of $RGO - ZnS$ composite, whereas it was only 34 % in presence of controlled-ZnS under similar experimental condition and same duration of time. The reduction kinetics are further articulated as

$$ln\left(\frac{C_0}{C}\right) \;=\; kt \tag{2.4.5}$$

where k is the reduction rate constant ($time^{-1}$). Figure 2.4.10B shows the linear variation of $ln\left(\frac{C_0}{C}\right)$ with time, demonstrating the occurrence of a pseudo-first order reduction kinetics of $4 - NP$.

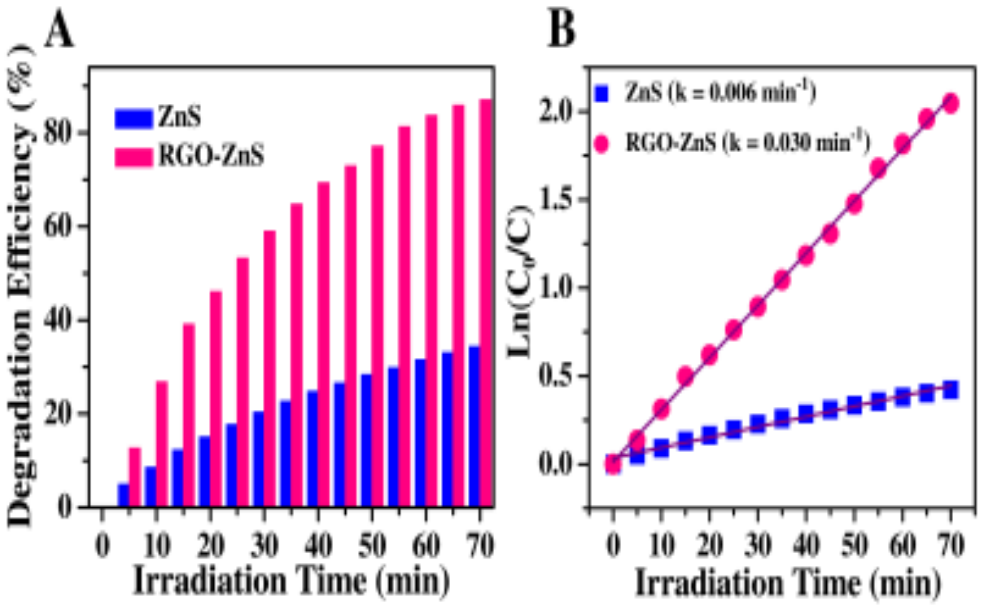

Figure 2.4.10: (A) The comparison of the photo reduction efficiency as a function of time under illumination over ZnS and $RGO - ZnS$. (B) Plot of $ln\,(C_0/C)$ as a function of irradiation time for the photocatalysis of $4 - NP$ solution containing ZnS and $RGO - ZnS$ composite.

The reduction rate constant of ZnS is $6 \times 10^{-3}\,min^{-1}$, whereas that of the $RGO - ZnS$ is $30 \times 10^{-3}\,min^{-1}$. This indicates the better efficiency of $RGO - ZnS$ catalyst compared to that of controlled-ZnS. The 5 times higher rates constant of $RGO - ZnS$ composite in compare to controlled-ZnS is due to the synergistic effect between RGO and ZnS with electronic communication, where RGO plays a vital role toward efficient photo induced charge separation and transportation. The photo induced electrons created in the high band gap ZnS nanorod transfers from its conduction band to the $LUMO$ level of $4 - NP$ through the RGO sheets, and will reduce the $4 - NP$ to 4-aminophenol $(4 - AP)$[212]. Simultaneously, the sacrificial donor $NaBH_4$ will fill the photoinduced holes at the valence band of ZnS

nanorod. The proposed reduction process of $4-NP$ to $4-AP$ is schematically presented in Figure 2.4.11.

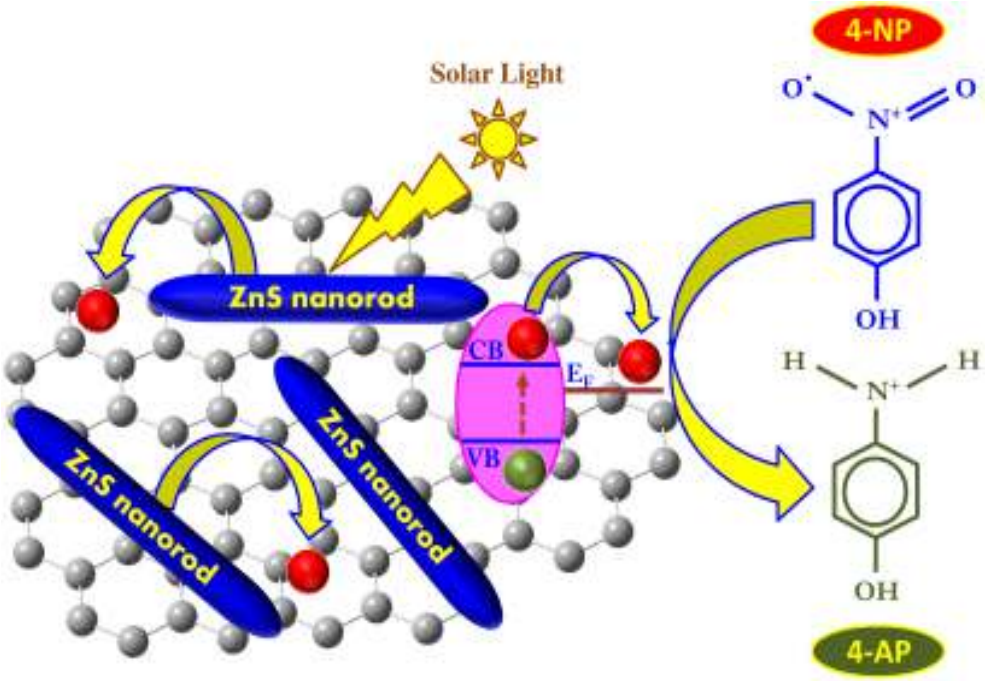

Figure 2.4.11: Schematic representation of reduction mechanism of 4-NP.

In addition, we have extended our work to study the variation of photoreduction efficiency for different weight ratios of RGO (varying from 0 to 20), keeping ZnS nanorod as constant. The photoreduction efficiency and the k for different weight ratios are presented in Figure 2.4.12A and 2.4.12B respectively.

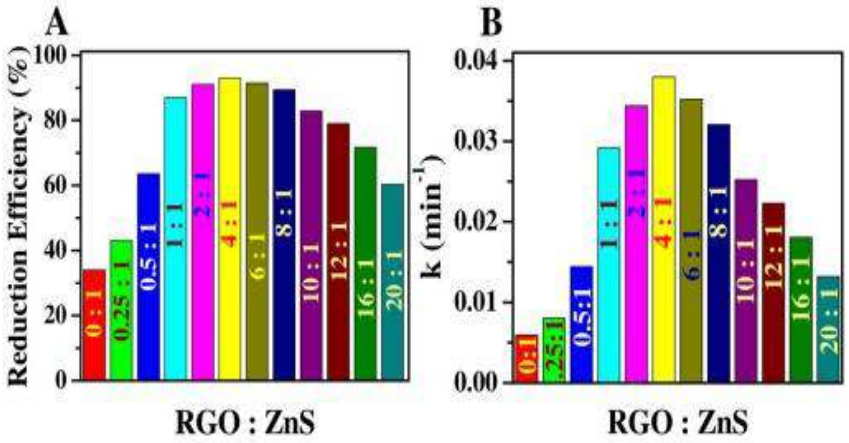

Figure 2.4.12: Variation of (A) reduction efficiency and (B) k with varying loading ratio of RGO in the $RGO - ZnS$ composite.

It is observed that both the parameters depend on the weight ratio of RGO and ZnS in the composite. The above observation opens up a new avenue for future research on the structural and functional correlation of the $RGO - ZnS$ composite towards the photocatalytic reduction of $4 - NP$.

The recycling test of photocatalysis of $RGO - ZnS$ was performed as shown in Figure 2.4.13A.

The recycle use of $RGO - ZnS$ composite does not markedly affect its photo reduction efficiency even after five cycles, which suggested that they had high stability and sustainability. The XRD pattern of $RGO - ZnS$ composite after five cycles of photocatalytic reactions (Figure 2.4.13B) reveals that the phase as well as structure remain unchanged. The XRD

result indicates that the $RGO - ZnS$ catalyst is sufficiently stable and not deactivated during the photocatalytic reduction of $4 - NP$ under simulated solar light illumination.

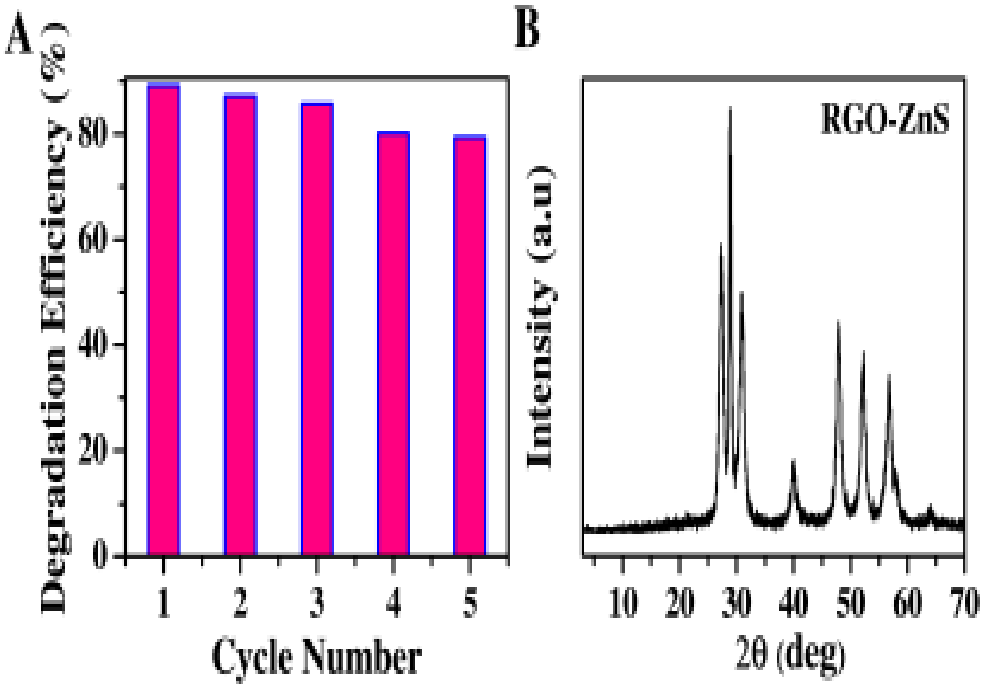

Figure 2.4.13: (A) Photoreduction efficiency of $RGO - ZnS$ composite for different cycle (B) The XRD pattern of $RGO - ZnS$ composite after five cycles of reduction of $4 - NP$.

2.5 Conclusions

$RGO - ZnS$ nanorod composite were synthesized successfully through a one pot single step solvothermal process. ZnS nanorod with length of $40 - 50\,nm$ were supported uniformly on RGO sheets without aggregation. The opto-electronic transport properties of large area solution processable $RGO - ZnS$ composite thin film device showed $37\,\%$ photosensitivity under $180\,mW cm^{-2}$

of simulated solar light intensity. The calculated time constant for growth and decay of our thin film device were $24\,s$ and $20\,s$ respectively. The $RGO - ZnS$ nanocomposite shows its superiority over controlled ZnS towards $4 - NP$ reduction under simulated solar light illumination. High photosensitivity and enhanced photocatalytic activity is mainly due to its superior adsorption capability, better absorption capacity of solar light, efficient charge separation and transportation between RGO and ZnS nanostructure. Thus our study not only lives up to its potential as a photo detector but also has a huge positive impact on toxic water pollutant removal.